



# Preparation of graphene oxide–cellulose acetate nanocomposite membrane for high-flux desalination

Yexun Shi<sup>1</sup>, Chang Li<sup>1</sup>, Dafang He<sup>1,2</sup>, Liming Shen<sup>1,\*</sup>, and Ningzhong Bao<sup>1,2,\*</sup>

<sup>1</sup> State Key Laboratory of Material-Oriented Chemical Engineering, College of Chemical Engineering, Nanjing Tech University, Nanjing, Jiangsu 210009, People's Republic of China

<sup>2</sup> Jiangnan Graphene Research Institute, Changzhou, Jiangsu 213149, People's Republic of China

Received: 25 May 2017

Accepted: 17 July 2017

Published online:  
24 July 2017

© Springer Science+Business  
Media, LLC 2017

## ABSTRACT

Graphene oxide–cellulose acetate (GO–CA) nanocomposite membranes have been successfully prepared via phase inversion method. The GO sheets were firstly well dispersed in formamide, and then the solution was mixed with acetone containing CA so as to confirm the GO sheets well dispersed in the final GO–CA nanocomposite membranes. All the GO–CA nanocomposite membranes are composed of dense skin layer and sponge-like sublayer. With the increase in GO contents (from 0 to 0.01 wt%), the skin layer gradually became thinner and the pore size in the sublayer increased; meanwhile, the contact angle of GO–CA membranes decreased from 70.59° to 53.42° due to better hydrophilicity. All the membranes, except for the nanocomposite membrane containing 0.01 wt% GO, have featured pores at about 0.9 nm. The permeation rate of the membrane containing 0.005 wt% GO was 2.3 times higher than that of the CA membrane (0 wt% GO) with a little decrease (~15%) in salt retention. Compared with CA membrane, the enhanced performance of GO–CA membranes may be attributed to their enhanced structure and hydrophilicity.

## Introduction

The freshwater shortage is getting globalized with the rapid growth of population and the vast pollution from industrialization [1]. To address the water crisis, several kinds of desalination technologies have been developed. As the world leading technology for desalination, reverse osmosis (RO) desalination process offers the highest energy efficiency for

producing freshwater from saline water [2–4]. In the RO process, reverse osmosis membrane acts as the semipermeable barrier, selectively allowing passage of water while partially or completely retaining salt. So far, a wide range of polymers have been used to prepare RO membranes, but the differences in chemical and physical properties limit the number used in practice [5]. Among these different polymeric materials, cellulose acetate (CA) is widespread due to

Yexun Shi and Chang Li have contributed equally.

Address correspondence to E-mail: lshen@njtech.edu.cn; nzhbao@njtech.edu.cn

its good desalination, excellent potential flux, low cost, and excellent hydrophilicity [3, 6–8].

In 1959, Reid and Breton [9] firstly demonstrated that CA symmetric membranes were capable of separating salt from water with 98% salt retention, although the water fluxes were less than  $10 \text{ mL m}^{-2} \text{ h}^{-1}$ . Until 1962, Loeb and Sourirajan [9] developed the first viable CA membrane with 99% salt retention and  $14.6 \text{ L m}^{-2} \text{ h}^{-1}$  water permeation at 100 bar, which made RO possible in practice. In this structure, CA asymmetric membranes have a dense thin skin layer supported on a thick micro-porous sublayer of the same polymer [10]. The dense skin layer plays a decisive role in membrane separation properties, which determines the flux and selectivity, while the thick micro-porous sublayer works exclusively as a mechanical support [11, 12].

As is known to all, the performance of RO membrane is rated by selectivity, chemical resistance, operational pressure differential, and the pure water permeability [13]. The GO asymmetric membrane with thin (from 0.1 to  $1 \mu\text{m}$ ) skin layer can largely reduce the resistance of the water transport, which provides a higher water flux than the initial symmetric membrane. However, the CA membranes undergo poor chemical resistance [14], bad thermal stability, and low antifouling properties, thus resulting in the short life of membranes and decreasing of membrane performance such as permeability and rejection [6, 15]. Therefore, extensive efforts have been spent to enhance their properties by adding additive into membranes [12, 16]. Thus far, various materials such as ZnO [8], carbon nanotubes (CNTs) [17],  $\text{Al}_2\text{O}_3$  [18] have been used to fabricate hybrid membranes to enhance their permeability and antifouling properties. Ahmad et al. [6] modified the CA/polyethylene glycol (PEG) membranes with varying amount of silica. The result indicated that the incorporation of  $\text{SiO}_2$  content could enhance the hydrophilicity and fouling resistance of membrane. The flux improved from  $0.35$  to  $2.46 \text{ L h}^{-1} \text{ m}^2$  along with an 11.41% relative increase in salt rejection. Abedini et al. [7] dispersed  $\text{TiO}_2$  nanoparticles in the CA casting solution and found out that the membrane became more porous, which led to an improved water permeation due to the increase in the mean pore size. Badawi et al. [9] successfully prepared CNT/CA nanocomposite membranes by phase inversion and observed a decrease in number of macrovoids with increase in the CNT content, which

consequently improved the permeation rate by 54% with 6% decrease in salt retention.

Graphene oxide (GO), as another type of promising nanomaterial, has been considered as a high-efficiency novel membrane material. Dai et al. [19] studied the permeation and ion rejection in layer-by-layer stacked GO nanochannels by using molecular dynamics (MD) simulation and found that laminate GO membranes with reasonable interlayer distances exhibit high ion rejection ability. Meanwhile, GO has also risen a research hotspot in hybrid membrane [20]. It has an effective thickness of 0.5 nm [21], and the lateral size is tunable from hundreds of nanometers up to tens of microns, making it an excellent candidate in composite membranes [22]. As a derivative of graphene, GO with oxygen-rich functional groups on its basal planes and edges can be manipulated in some solution [23]. Based on its admirable hydrophilicity, GO-polymer membrane materials could ensure high water permeation and impede biofouling [24]. Wang et al. [25] prepared GO-blended PVDF membranes, and the contact angle decreased from  $79.2^\circ$  to  $60.7^\circ$ , which implied an improved antifouling ability. Choi et al. [26] coated GO on the surface of polyamide (PA) thin-film composite (TFC) membrane via layer-by-layer deposition, and the resulted GO coating layer could increase the surface hydrophilicity and reduce the surface roughness, leading to the improved antifouling performance. Furthermore, GO exhibits lots of extraordinary physicochemical properties such as good mechanical properties and thermo-mechanical stability. In previous studies, Zhang and Jiang [27] performed systematic MD simulations to elucidate the mechanical properties of graphene/GO paper-based polymer composites and found the macroscopic mechanical response was controlled by the H-bond networks formed between the GO sheets and polymer molecules. Kabiri and Namazi [28] synthesized the CA-GO nanocomposite films with 63.88 and 61.92% increase in Young's modulus and tensile strength, respectively. Uddin et al. [29] prepared reduced graphene oxide (rGO)/CA nanocomposite film and discovered that the tensile strength and modulus were, respectively, improved by 120 and 145% with increasing rGO loading. Nevertheless, many factors can affect the final properties and applications of GO/polymer composites, especially the dispersion state of GO in the polymer matrix [30, 31]. Homogeneous dispersion of GO plays the

key role in the performance of composites, and the small-size GO (<5 $\mu$ m) normally has remarkable dispersion, which improves interfacial contact with the polymer matrix and contributes to a homogeneous morphology with ridge-and-valley structures [13].

The aim of this work is to make GO evenly dispersed in casting solution, so as to obtain homogeneous GO–CA nanocomposite RO membranes for desalination and improve their performance. The membranes were developed by phase inversion technique [32] with the casting solution component of 25 wt% cellulose acetate, 45 wt% acetone, 30 wt% formamide with different GO content. The influence of different masses of GO (0.0001, 0.0005, 0.001, 0.005, and 0.01 wt%) on the morphology and pore size of GO–CA nanocomposite membranes was investigated. In addition, the performance of permeability and salt retention were studied.

## Experimental

### Materials

Cellulose acetate (CA) with an average molecular weight of 50000 Da and 39.8 wt% acetyl content was obtained from Eastman Chemical Company. Natural flake graphite with a size of around 150  $\mu$ m was purchased from Qingdao Meizhen Company. Acetone (AC, purity  $\geq$ 99.5%), formamide (FA, purity  $\geq$ 99.5%), potassium permanganate (KMnO<sub>4</sub>, 99.5%, analytical grade), potassium nitrate (99.5%, analytical grade), sulfuric acid (98%), and hydrogen peroxide aqueous solution (30%) were bought from Shanghai Lingfeng Chemical Reagents Company. All chemicals were used as received.

### Synthesis of graphene oxide sheets

GO was synthesized by improved Hummers' method [33]. In a typical synthetic procedure, natural graphite (1.0 g) with average size of 100 mesh and potassium nitrate (1.5 g) were mixed in H<sub>2</sub>SO<sub>4</sub> (50 mL, 98 wt%) with stirring; and then potassium permanganate (6.0 g) was slowly added into the mixture with vigorous stirring. The above mixing steps were carried out in an ice bath to keep the temperature below 20 °C. The mixture was then kept at 45 °C for 2 h in a water bath, forming a thick paste,

before heated to 90 °C. 100 mL water was gradually added to the paste at 90 °C with constant agitation for 10–20 min. Additional 200 mL water was subsequently added into the mixture in a similar fashion. At last, the mixture was treated with 10 mL H<sub>2</sub>O<sub>2</sub> (30 wt%) at room temperature and the color of the solution immediately turned to golden yellow. After repeated centrifugation and washing with DI water, the pH of the solution eventually became neutral. The resulting graphite oxide was then dispersed in deionized (DI) water to form a suspension. By ultrasonic treatment, the graphite oxide was transformed into graphene oxide (GO). In order to obtain small lateral size, the ultrasonic process lasted for 12 h. Then the dispersion was transferred into a culture dish. After freeze-dried by liquid nitrogen, the frozen dispersion was freeze-dried for 72 h to get loosely packed GO sheets.

### Preparation of GO/formamide, CA/acetone, and casting solutions

Preparation of GO/formamide solution: The GO powders were dispersed in formamide (30 wt%) with different concentrations of 0.0001, 0.0005, 0.001, 0.005, and 0.01 wt%, and the solutions were sonicated for 2 h to form homogeneous GO/formamide suspensions. For comparison, the GO/acetone suspension (containing 0.0001 wt% GO) was prepared by dispersing GO powders in acetone (45 wt%). The GO/formamide/acetone solution was prepared by adding acetone (45 wt%) into the homogenous GO/formamide solution, while the GO/acetone/formamide solution was prepared by adding formamide (30 wt%) into the GO/acetone suspension.

Preparation of CA/acetone solution: CA (25 wt%) was added into acetone (45 wt%) with vigorous stirring for 24 h to form a homogenous solution.

Preparation of casting solution: The GO/formamide (30 wt%) dispersions with different GO contents were mixed with CA/acetone solutions (70 wt%) to form casting solution. The agitation was conducted for 24 h to have optimal dispersion of GO in the polymer solutions. The casting solution was left at room temperature for 12 h to allow any air bubbles to dissipate. A negative control casting solution was prepared by mixing the GO/acetone solution and CA (25 wt%), vigorous stirring for 24 h, and then adding formamide (30 wt%) into the

solution. The negative control casting solution contains 25 wt% CA, 30 wt% formamide, and 45 wt% GO/acetone solution with 0.0001 wt% GO.

### Preparation of GO–CA membranes

All the membranes were prepared by the classical phase inversion method using distilled water as the nonsolvent coagulation bath at 5 °C. The casting solution was quickly spread on a glass substrate at room temperature, and then the cast membrane was left in air for 30 s for the evaporation of solvent within the skin layer before immersed into water bath. The membranes were maintained in water for more than 2 h to ensure adequate phase transformation, followed by a post-treatment at 85 °C for 5 min. Finally, the membranes were rinsed in distilled water before characterization. The negative control membrane is named as GO-Neg membrane for discussion.

### Material and membrane characterizations

The dispersion of GO sheets in formamide and acetone was characterized by photography. The thickness of GO sheets was obtained by atomic force microscopy (AFM, Bruker ICON). The morphology and microstructure of membrane cross section were determined by field emission scanning electron microscopy (FESEM, HITACHI S-4800). The  $N_2$  adsorption–desorption was performed at 77 K on a Belsorp-max. The pore size distribution was calculated from adsorption branches using the Horváth–Kawazoe (HK) method. The contact angle of a 5  $\mu$ L water droplet on the membrane surface was recorded by a KRÜSS DSA100 (KRÜSS, Germany) contact angle system at ambient temperature.

Reverse osmosis experiments were conducted in a stainless steel module, and the apparatus is schematically illustrated in Fig. 1. The membranes were cut into a disk shape and installed in the membrane cell with effective area of 12.56 cm<sup>2</sup>. The feed tank was filled with a 2000 ppm NaCl solution. The permeation rate at an operating pressure of 30 bar was calculated using Eq. (1) as follows:

$$\text{Flux} = \frac{Q}{A \cdot \Delta t} \quad (1)$$

where  $Q$  is the permeate quantity (L),  $A$  is the effective membrane area (m<sup>2</sup>), and  $\Delta t$  is the sampling time (h).

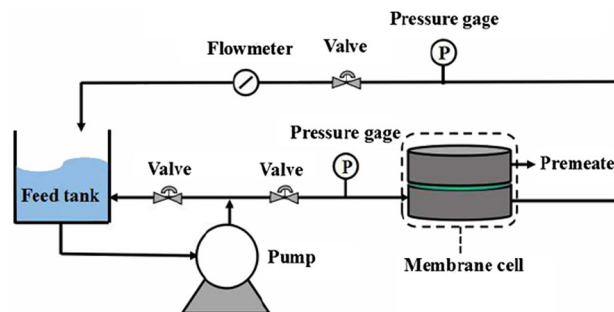


**Figure 1** Schematic illustration of the apparatus for reverse osmosis experiments.

The salt retention rate was calculated by the feed and permeate concentrations using Eq. (2) as follows:

$$R(\%) = \frac{C_f - C_p}{C_f} \times 100\% \quad (2)$$

where  $R$  is the salt retention rate,  $C_f$  is the feed concentration (ppm), and  $C_p$  is the salt permeate concentration (ppm).

## Results and discussion

### Dispersion of the GO sheets in GO/formamide and GO/acetone solutions

The casting solution used in this work was firstly prepared by Manjikian et al. [34]. In this recipe, acetone and formamide were used as solvent and swelling agent, respectively. However, the dispersion of GO in acetone was so poor that GO cannot work. In order to solve this problem and prevent the change of the composition, the GO sheets were firstly dispersed in formamide and then mixed with acetone. We have compared the stability of GO/formamide and GO/acetone solutions. Figure 2a shows the two solutions right after the 2-h ultrasonic treatment. The GO/formamide solution is much more limpid than the GO/acetone solution. The black line drawn on the back side of the bottle is clearly visible through the GO/formamide solution, but that is completely blocked by the GO/acetone solution. After the two solutions were placed for 5 h, the GO/formamide solution did not show much difference, while the GO sheets in acetone were completely precipitated at the bottom of bottle, as shown in Fig. 2b. The aggregation of GO sheets in solvent was irreversible, as shown in Fig. 2c–d. The later introduction of acetone into the homogeneous GO/formamide suspension did not

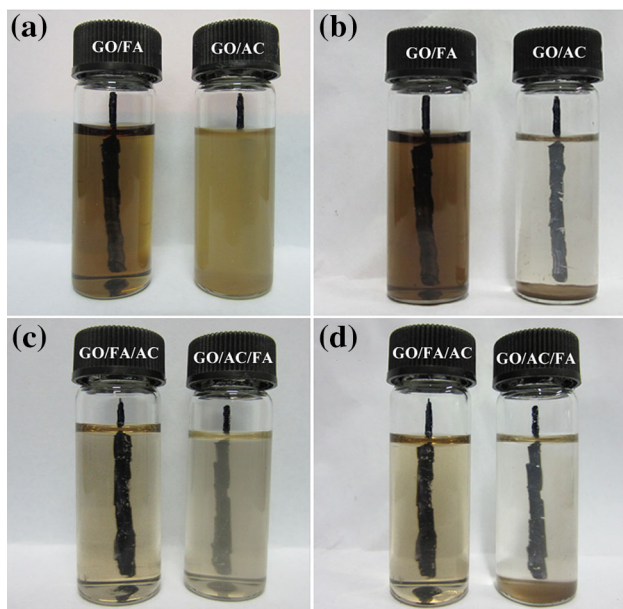


**Figure 2** Optical images of GO/formamide (GO/FA) and GO/acetone (GO/AC) solutions, taken **a** right after the ultrasonic treatment and **b** 5 h after the ultrasonic treatment; optical images of GO/formamide/acetone (GO/FA/AC) and GO/acetone/formamide (GO/AC/FA) solutions, taken **c** right after the ultrasonic treatment and **d** 5 h after the ultrasonic treatment. The black lines were drawn on the back side of bottles.

affect the dispersion of GO sheets. The GO/formamide/acetone solution maintained a good dispersion state even after placed for 5 h. Similarly, the folded and reunited GO sheets in acetone cannot be exfoliated again by adding formamide into the GO/acetone solution. The GO sheets completely precipitated in the GO/acetone/formamide solution after placed for 5 h. To sum up, the first well dispersion in formamide can effectively improve the dispersion in acetone so as to make sure the GO sheets play their full roles in the casting solution.

The morphologies of GO sheets in both formamide and acetone were examined by AFM. The two solutions were deposited on a freshly cleaved mica surface through a drop-casting method. Figure 3 shows AFM images and height profiles of GO sheets in the GO/formamide and GO/acetone solutions. The GO sheets dispersed in formamide (Fig. 3a) still have the lamellar structure with the thickness of 1–2 nm (Fig. 3c), which indicates the existence of single-layer GO sheet. On the contrary, the thickness of GO sheets dispersed in acetone (Fig. 3b) is about 20 nm or even more than 40 nm (Fig. 3d), which indicates the severe agglomeration of GO sheets. The polarity parameters

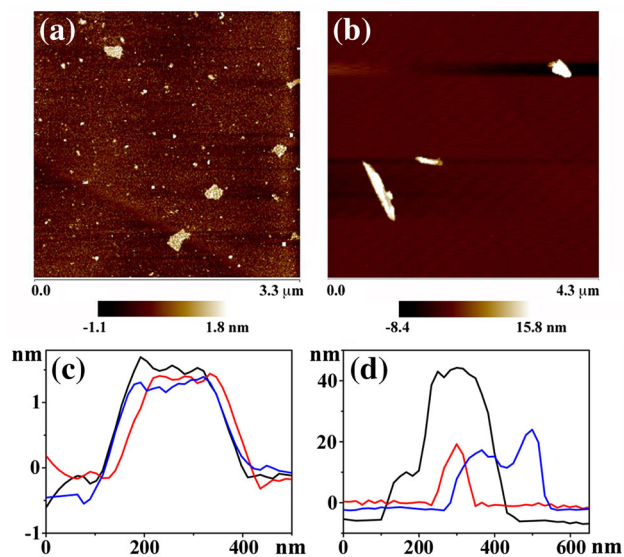


**Figure 3** **a, c** AFM image and height profile of GO sheets in GO/formamide solution; **b, d** AFM image and height profile of GO sheets in GO/acetone solution.

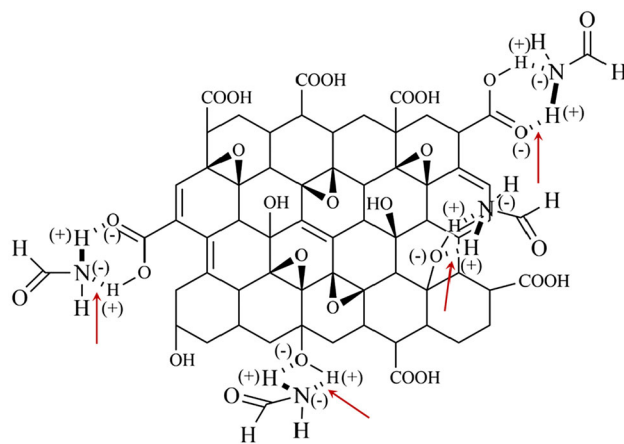


**Figure 4** Schematic illustration of hydrogen bonds between formamide and functional groups of GO sheets.

of water, formamide, and acetone are 10.2, 9.6, and 5.4, respectively. Compared to acetone, the polarity of formamide is closer to the water. It has been reported that GO surface contains several functional groups including epoxide, hydroxyl, and carboxyl groups and can be well dispersed in water and N, N-dimethylformamide without any assistance of chemical functionalization [35, 36]. Like water, formamide can lead to the formation of hydrogen bonds (illustrated in Fig. 4) with the functional groups in GO sheets, which makes the GO/formamide solution stable. The lateral size of GO sheets in the GO/formamide solution is about 300 nm (Fig. 3c), a little bit

smaller than others reported [37, 38]. The small size of GO sheets is caused by the ultrasonic treatments during the preparation process of GO sheets and GO/formamide solution. Compared to large GO sheets that are easy to wrinkle during phase inversion, small GO sheets are considered to have more advantages of playing their roles in membranes.

### Structure and properties of the GO-CA membranes

The structure of membranes is strongly influenced by the uniform dispersion of GO sheets. The cross-sectional morphologies of membranes are presented in Fig. 5. The GO-CA membrane consists of a dense skin layer and a spongeous support layer (Fig. 5a), while the GO-Neg membrane contains many finger-like pores (Fig. 5b). The above results indicate that a low GO content could have close influence on the morphologies of sublayer. The finger-like pores were

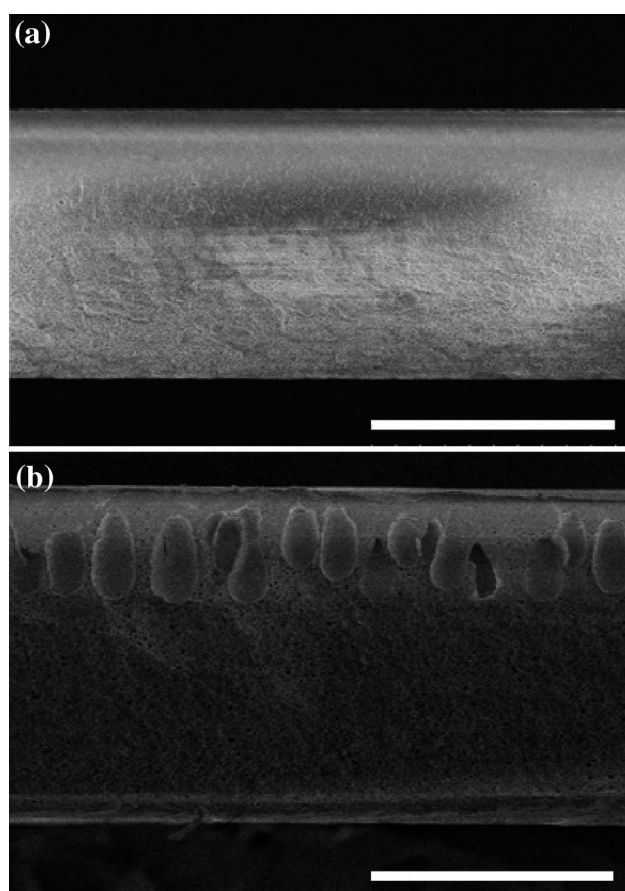


**Figure 5** Cross-sectional SEM images of **a** 0.0001 wt% GO-CA membrane and **b** GO-Neg membrane. The scale bars present 100  $\mu\text{m}$ .

caused by instantaneous demixing, and the fast solvent-nonsolvent exchange resulted in the emergence of large pores in the phase inversion process [39]. It was reported that the salt rejection of finger-like pores is lower than that of spongeous pores [11]. A more porous macrovoid sublayer is always accompanied by a less dense top surface layer, and thus the finger-like pores in the GO-Neg membrane implicate massive amount of large pores residing in the sublayer, which is not favored for the reverse osmosis process under high pressure.

The presence of GO can promote the phase separation in the coagulation bath. Smolders et al. [32] explained that GO sheets, acting as a hydrophilic additive with nonsolvent properties, can increase the thermodynamic instability of the cast film and locally induce nucleation which expands the pore size. Baldino et al. [40] confirmed that the mean pore size increased from 9.2 to 16.6  $\mu\text{m}$  by increasing the GO amount up to 9%. Therefore, fabrication of GO-CA membranes with adjustable amount of homogeneously dispersed GO sheets is a promising strategy for making efficient reverse osmosis membranes with high permeation rates and good salt rejection.

The content of GO in GO-CA membranes was systematically adjusted to study the structural evolution of the reverse osmosis membranes. Figure 6a–f shows the cross-sectional SEM images of the GO-CA membranes with different GO contents in the range of 0, 0.0001, 0.0005, 0.001, 0.005, and 0.01 wt%. There is no finger-like pore observed in all of these membranes, and the structure of all the six membranes can be treated as a dense top layer and a spongeous support layer for easy observation and discussion. Among the six samples, the pure CA membrane (Fig. 6a) exhibits the least porous structure in the sublayer which always accompanied by a dense top layer structure. With increasing the GO content, there is a noticeable size increase in spongeous pores in the sublayer. Accordingly, the membranes tend to be more porous and the top layers become thinner because the hydrophilic GO can accelerate the rate of solvent-nonsolvent exchange and eventually lead to the emergence of instantaneous demixing, which means the polymer precipitates and solid film is formed very rapidly after immersion in the nonsolvent bath. This type of demixing generally results in finger-like macrovoids and finely thin skin layer [39]. However, in our experiment, GO is well dispersed and the addition is very little. So the increase in GO

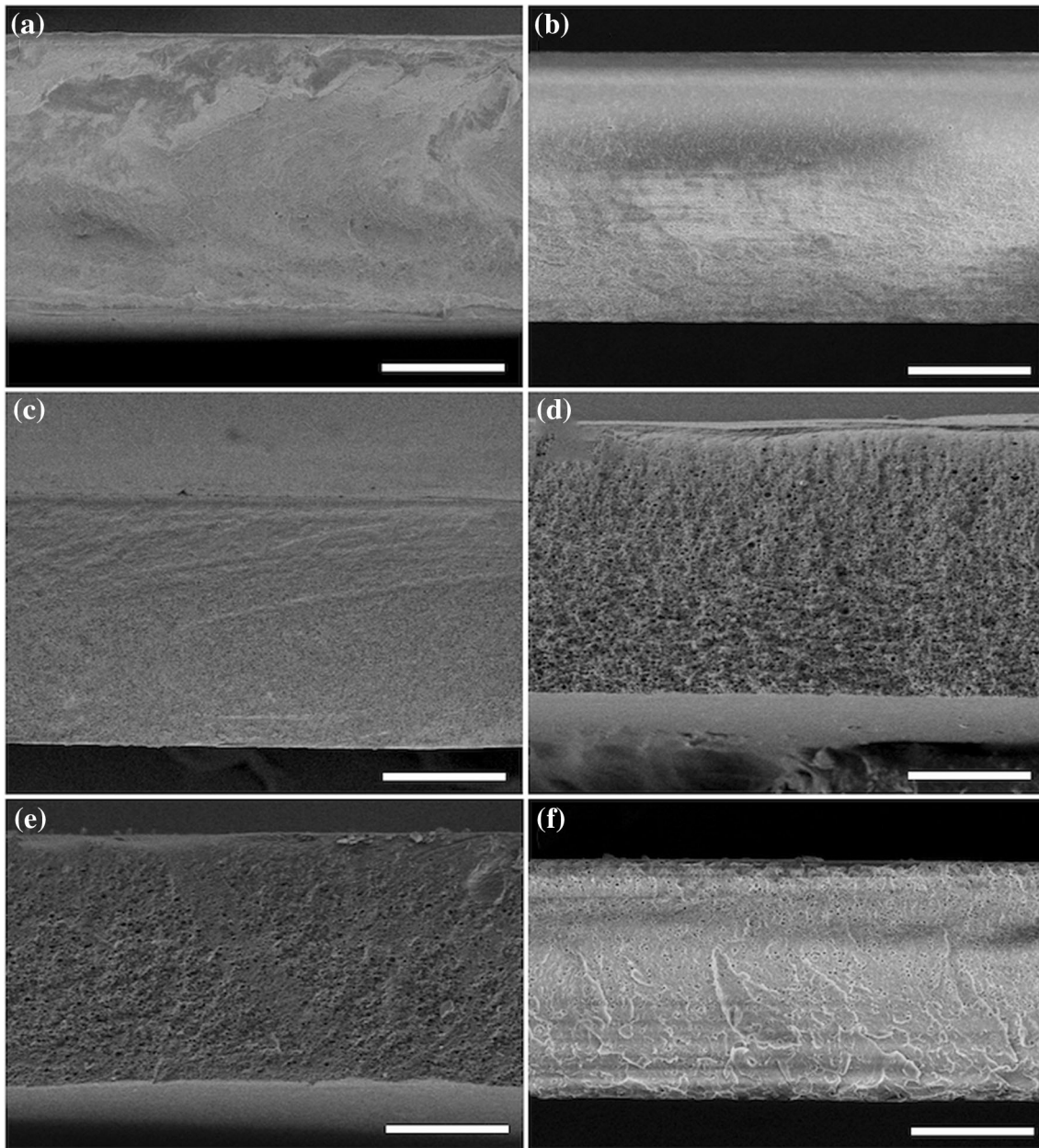


**Figure 6** Cross-sectional SEM images of the GO–CA membranes with different GO contents of **a** 0, **b** 0.0001, **c** 0.0005, **d** 0.001, **e** 0.005, and **f** 0.01 wt%. The *scale bars* present 50  $\mu\text{m}$ .

content can only increase the pore size and decrease the thickness of top layer without any changes in membrane morphology (sponge-like pores in sub-layer). When the amount of GO is increased to 0.01 wt%, the dense top layer disappears and the pores in sublayer are larger than the other ones (Fig. 6f). If we continue to increase the GO content, the finger-like pores will form due to the instantaneous demixing even though the GO is well dispersed.

The pore size distributions of the six samples are plotted in Fig. 7. As shown in Fig. 7a, the pure CA membrane has sharp featured peaks at 0.7 and 0.9 nm. After the addition of GO sheets, the featured peak of 0.7 nm pores immediately becomes weak or almost disappears. The peak of 0.9 nm pores gets slightly broader and stronger in the 0.0001 wt% GO–CA membrane (Fig. 7b), and then the peak density starts to decrease from the 0.0005 to the 0.005 wt%

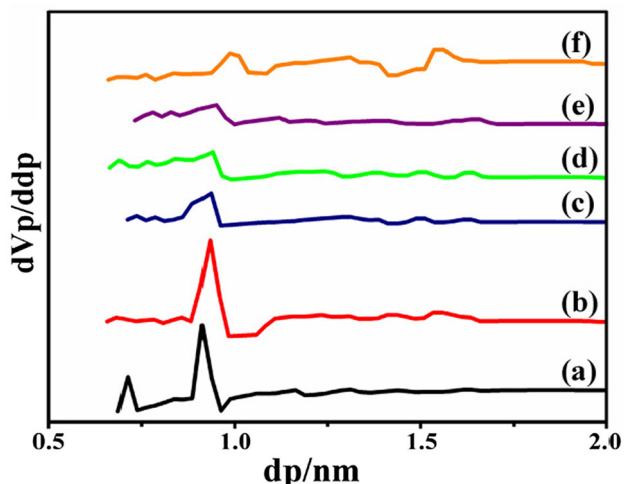


**Figure 7** Pore size distribution plots of the GO–CA membranes with different GO contents of *a* 0, *b* 0.0001, *c* 0.0005, *d* 0.001, *e* 0.005, and *f* 0.01 wt%.

GO–CA membrane (Fig. 7c–e). In the 0.01 wt% GO–CA membrane (Fig. 7f), two new peaks at 1.0 and 1.6 nm, instead of 0.7 and 0.9 nm, are observed. The pore size distribution of six samples indicates that the pure CA sample has the most dense structure with pore size concentrated at 0.7 and 0.9 nm, the pore size gets more uniform around 0.9 nm and the porosity of the GO–CA membranes increases with the addition of GO sheets, and the effective top layer can be destroyed after the GO content reaches 0.01 wt%. Figure 8 presents the BET surface area of the six membranes. The pure CA membrane has a relatively higher value due to concentrated pores of 0.7 and 0.9 nm in size. The large decrease in surface area from the 0 to the 0.0005 wt% GO–CA membrane is dominated by the enlarged pores size. With the

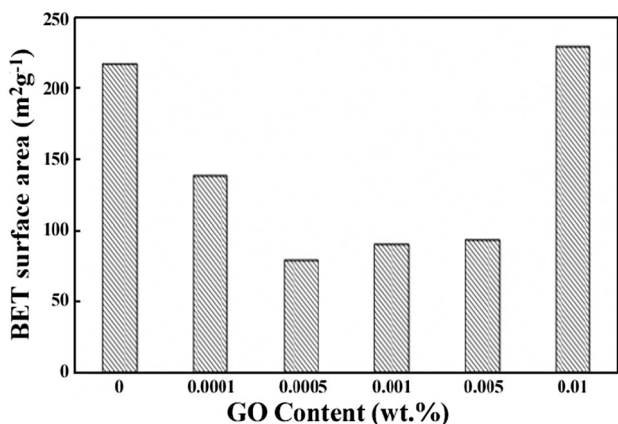


**Figure 8** BET surface areas of GO–CA membranes containing different contents of GO.

increase in pore size, the hydrophilic GO destroys the original dense porous structure. The large pores squeeze the small ones, resulting in a significant decrease in the pore volume (from 0.4825 to 0.3133 cm<sup>3</sup> g<sup>-1</sup>) and the surface area (from 217.42 to 78.859 m<sup>2</sup> g<sup>-1</sup>). From the 0.0005 to the 0.005 wt% GO–CA membrane, there is a small increase observed in the surface area. The pore size distribution does not change a lot within the range (Fig. 7c–e), but the pore volume increases much (from 0.3133 to 0.4492 cm<sup>3</sup> g<sup>-1</sup>) due to the increase in the number of large pores. When the GO addition increases to 0.01 wt%, the further increase in pore size and pore volume (from 0.4492 to 0.5319 cm<sup>3</sup> g<sup>-1</sup>) makes the film have the highest surface area.

The hydrophilicity of membrane has a great influence on the membrane permeation rate and is usually characterized by the measurement of water contact angle. As shown in Fig. 9, the water contact angles of the 0, 0.0001, 0.0005, 0.001, 0.005, and 0.01 wt% GO–CA membranes are 70.59°, 69.69°, 65.43°, 63.83°, 59.88°, and 53.42°, respectively. The gradual decline of the water contact angle indicates that the hydrophilicity is improved by the addition of GO sheets. The GO sheets contain surface hydrophilic groups that can enhance the hydration effect with water and thus intrinsically increase the hydrophilicity of the membrane. The addition of GO sheets also affects the surface characters such as roughness, porosity, and pore size distribution of the membrane. As indicated by the Cassie’s law, for the hydrophilic surface with contact angle less than 90°, the apparent contact angle decreases with the increase in surface roughness [41]. The SEM images

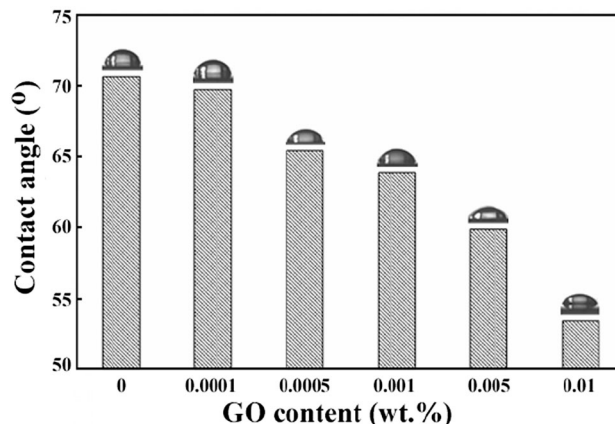


**Figure 9** Contact angles of GO–CA membranes containing different contents of GO.



(Fig. 6) show that the porosity of the GO–CA membranes increases along with the increments of GO content which can enhance the wettability of the membranes. Thus, the GO sheets intrinsically and externally contribute to the hydrophilicity of membranes.

### Performance of the GO–CA membranes

Figure 10 displays the permeability and salt rejection of the six membranes. The plotted lines clearly show that with the addition of GO sheets to the membranes, the permeation has a significant increase with a reasonable loss of retention. The pure CA membrane exhibits the lowest water flux ( $5.96 \text{ L m}^2 \text{ h}^{-1}$ ) and the highest salt rejection (97.85%). This is consistent with its most dense structure among the six samples. When the GO content increased to 0.001 wt%, the water flux increased to  $11.16 \text{ L m}^2 \text{ h}^{-1}$  (increased by 87.25% compared with the pure CA), with a very small drop of salt rejection (5.62%). In general, the flux of RO membrane will enhance as a consequence of improved hydrophilicity, because the interaction between the membrane surface and water molecules is enhanced via hydrogen bonding and/or electrostatic attraction [41, 42]. The GO sheets not only increased the hydrophilicity of membranes, but also improved their porosity and uniformed pore distribution, thus significantly improved the permeability with a small loss of rejection. When the GO content increased to 0.005 wt%, the water flux increased to  $13.65 \text{ L m}^2 \text{ h}^{-1}$  (improved by 129%) and

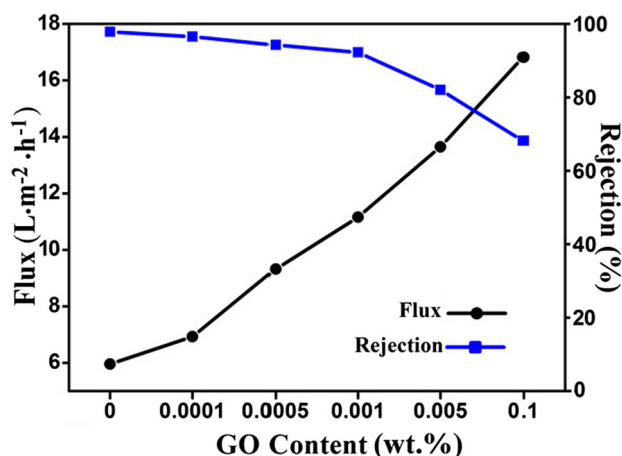


**Figure 10** Water fluxes and 2000 ppm salt rejections of GO–CA membranes containing different contents of GO under 30 bar operation pressure.

the salt rejection dropped by 15.82% (from 97.85 to 82.03%). The decrease in the salt rejection was caused by the surface defects, namely some large pores came up to the surface of skin layer. The 0.005 wt% seemed to be a boundary content, and the rejection dropped quickly with additional GO introduction. The 0.01 wt% GO–CA membrane showed the highest water flux ( $16.82 \text{ L m}^2 \text{ h}^{-1}$ ) because of its best hydrophilicity and highly porous structure, but the loss of dense skin layer resulted in almost 30% loss of salt rejection. Therefore, the GO–CA membrane with 0.005 wt% GO content is the optimal reverse osmosis membrane with  $13.65 \text{ L m}^2 \text{ h}^{-1}$  water flux and 82.03% salt rejection.

### Conclusion

In conclusion, we have successfully prepared a high-flux CA nanocomposite membrane modified by well-dispersed GO sheets via phase inversion technique. The structure of GO–CA membranes has been controlled by the demixing rate, and GO, as a hydrophilic additive, can locally induce nucleation which expands the pore size. In addition, the GO works only when it is well dispersed. With a favorable dispersion, even a small amount of GO sheets can cause a great change in membrane performance. By adjusting the GO content, the pore size distribution and the hydrophilicity of membranes have been optimized. The 0.005 wt% GO–CA membrane has a water permeation of  $13.65 \text{ L m}^2 \text{ h}^{-1}$  at 30 bar operation pressure, 129% higher than that of a pure CA membrane with a small decline of salt rejection.

### Acknowledgements

This research was supported by National Key Technology Research and Development Program (No. 2014BAE12B0104), the National Natural Science Foundation of China (No. 51425202), Natural Science Foundation of Jiangsu Province (BK20160093) and the Industrial Support Program of Changzhou (No. CE20160031).

### Compliance with ethical standards

**Conflict of interest** The authors declare there are no conflicts of interest regarding the publication of this paper.

## References

- [1] Greenlee LF, Lawler DF, Freeman BD et al (2009) Reverse osmosis desalination: water sources, technology, and today's challenges. *Water Res* 43:2317–2348
- [2] Mezher T, Fath H, Abbas Z et al (2011) Techno-economic assessment and environmental impacts of desalination technologies. *Desalination* 266:263–273
- [3] Ferjani E, Lajimi RH, Deratani A et al (2002) Bulk and surface modification of cellulose diacetate based RO/NF membranes by polymethylhydrosiloxane preparation and characterization. *Desalination* 146:325–330
- [4] Arthanareeswaran G, Thanikaivelan P, Srinivasan K et al (2004) Synthesis, characterization and thermal studies on cellulose acetate membranes with additive. *Eur Polym J* 40:2153–2159
- [5] Saljoughi E, Sadrzadeh M, Mohammadi T (2009) Effect of preparation variables on morphology and pure water permeation flux through asymmetric cellulose acetate membranes. *J Membr Sci* 326:627–634
- [6] Ahmad A, Waheed S, Khan SM et al (2015) Effect of silica on the properties of cellulose acetate/polyethylene glycol membranes for reverse osmosis. *Desalination* 355:1–10
- [7] Abedini R, Mousavi SM, Aminzadeh R (2011) A novel cellulose acetate (CA) membrane using TiO<sub>2</sub> nanoparticles: preparation, characterization and permeation study. *Desalination* 277:40–45
- [8] Ali M, Zafar M, Jamil T et al (2011) Influence of glycol additives on the structure and performance of cellulose acetate/zinc oxide blend membranes. *Desalination* 270:98–104
- [9] El Badawi N, Ramadan AR, Esawi AMK et al (2014) Novel carbon nanotube-cellulose acetate nanocomposite membranes for water filtration applications. *Desalination* 344:79–85
- [10] Mohammadi T, Saljoughi E (2009) Effect of production conditions on morphology and permeability of asymmetric cellulose acetate membranes. *Desalination* 243:1–7
- [11] Wang Z, Ma J, Liu Q (2011) Pure sponge-like membranes bearing both high water permeability and high retention capacity. *Desalination* 278:141–149
- [12] Chuang WY, Young TH, Chiu WY et al (2000) The effect of polymeric additives on the structure and permeability of poly(vinyl alcohol) asymmetric membranes. *Polymer* 41:5633–5641
- [13] Chae H, Lee J, Lee C et al (2015) Graphene oxide-embedded thin-film composite reverse osmosis membrane with high flux, anti-biofouling, and chlorine resistance. *J Membr Sci* 483:128–135
- [14] El-Saied H, Basta AH, Barsoum BN et al (2003) Cellulose membranes for reverse osmosis Part I. RO cellulose acetate membranes including a composite with polypropylene. *Desalination* 159:171–181
- [15] Rustemeyer P (2004) History of CA and evolution of the markets. *Macromol Symp* 208:1–6
- [16] Kim Y, Noh Y, Lim EJ et al (2014) Star-shaped Pd@Pt core-shell catalysts supported on reduced graphene oxide with superior electrocatalytic performance. *J Mater Chem A* 2:6976–6986
- [17] Sabir A, Shafiq M, Islam A et al (2015) Fabrication of tethered carbon nanotubes in cellulose acetate/polyethylene glycol-400 composite membranes for reverse osmosis. *Carbohydr Polym* 132:589–597
- [18] Wang Y, Yang L, Luo G et al (2009) Preparation of cellulose acetate membrane filled with metal oxide particles for the pervaporation separation of methanol/methyl tert-butyl ether mixtures. *Chem Eng J* 146:6–10
- [19] Dai HW, Xu ZJ, Yang XN (2016) Water permeation and ion rejection in layer-by-layer stacked graphene oxide nanochannels: a molecular dynamics simulation. *J Phys Chem C* 120:22585–22596
- [20] Sun P, Zhu M, Wang K et al (2013) Selective ion penetration of graphene oxide membranes. *ACS Nano* 7:428–437
- [21] Medhekar NV, Ramasubramaniam A, Ruoff RS et al (2010) Hydrogen bond networks in graphene oxide composite paper: structure and mechanical properties. *ACS Nano* 4:2300–2306
- [22] Aba NFD, Chong JY, Wang B et al (2015) Graphene oxide membranes on ceramic hollow fibers—microstructural stability and nanofiltration performance. *J Membr Sci* 484:87–94
- [23] Dreyer DR, Park S, Bielawski CW et al (2010) The chemistry of graphene oxide. *Chem Soc Rev* 39:228–240
- [24] Lee J, Chae H, Won YJ et al (2013) Graphene oxide nanoplatelets composite membrane with hydrophilic and antifouling properties for wastewater treatment. *J Membr Sci* 448:223–230
- [25] Wang Z, Yu H, Xia J et al (2012) Novel GO-blended PVDF ultrafiltration membranes. *Desalination* 299:50–54
- [26] Choi W, Choi J, Bang J et al (2013) Layer-by-Layer assembly of graphene oxide nanosheets on polyamide membranes for durable reverse-osmosis applications. *ACS Appl Mater Inter* 5:12510–12519
- [27] Zhang JW, Jiang DZ (2014) Molecular dynamics simulation of mechanical performance of graphene/graphene oxide paper based polymer composites. *Carbon* 67:784–791
- [28] Kabiri R, Namazi H (2014) Nanocrystalline cellulose acetate (NCCA)/graphene oxide (GO) nanocomposites with

- enhanced mechanical properties and barrier against water vapor. *Cellulose* 21:3527–3539
- [29] Uddin ME, Layek RK, Kim HY et al (2016) Preparation and enhanced mechanical properties of non-covalently-functionalized graphene oxide/cellulose acetate nanocomposites. *Compos Part B-Eng* 90:223–231
- [30] Wang C, Lan Y, Yu W et al (2016) Preparation of amino-functionalized graphene oxide/polyimide composite films with improved mechanical, thermal and hydrophobic properties. *Appl Surf Sci* 362:11–19
- [31] Nguyen DL, Hippi U, Korhonen JT et al (2011) Enhanced mechanical and electrical properties of polyimide film by graphene sheets via in situ polymerization. *Polymer* 52:5237–5242
- [32] Smolders CA, Reuvers AJ, Boom RM (1992) Microrstructures in phase-inversion membranes. 1. formation of macrovoids. *J Membr Sci* 73:259–275
- [33] He D, Shen L, Zhang X et al (2014) An efficient and eco-friendly solution-chemical route for preparation of ultra-stable reduced graphene oxide suspensions. *AIChE J* 60:2757–2764
- [34] Manjikian S, Loeb S, Mccuchan JW (1965) Proceedings of first international desalination symposium, vol 2. Washington, DC, pp 159–173
- [35] Cai D, Song M, Xu C (2008) Highly conductive carbon-nanotube/graphite-oxide hybrid films. *Adv Mater* 20:1706
- [36] Cai D, Song M (2007) Preparation of fully exfoliated graphite oxide nanoplatelets in organic solvents. *J Mater Chem* 17:3678–3680
- [37] Zhang J, Yang H, Shen G et al (2010) Reduction of graphene oxide via L-ascorbic acid. *Chem Commun* 46:1112–1114
- [38] Zhang X, Liu Y, Sun C et al (2015) Graphene oxide-based polymeric membranes for broad water pollutant removal. *RSC Adv* 5:100651–100662
- [39] Guillen GR, Pan Y, Li M et al (2011) Preparation and characterization of membranes formed by nonsolvent induced phase separation: a review. *Ind Eng Chem Res* 50:3798–3817
- [40] Baldino L, Sarno M, Cardea S et al (2015) Formation of cellulose acetate-graphene oxide nanocomposites by supercritical CO<sub>2</sub> assisted phase inversion. *Ind Eng Chem Res* 54:8147–8156
- [41] Lalia BS, Kochkodan V, Hashaikeh R et al (2013) A review on membrane fabrication: structure, properties and performance relationship. *Desalination* 326:77–95
- [42] Li Q, Pan X, Hou C et al (2012) Exploring the dependence of bulk properties on surface chemistries and microstructures of commercially composite RO membranes by novel characterization approaches. *Desalination* 292:9–18